Magnetic Fabry-Perot Interferometer For Valley Filtering In Silicene

M.Sc. THESIS

by

Palzor Lepcha

(Roll No.-2103151019)

to

DEPARTMENT OF PHYSICS

INDIAN INSTITUTE OF TECHNOLOGY INDORE

INDORE - 453 552, INDIA

June, 2023

Magnetic Fabry-Perot Interferometer For Valley Filtering In Silicene

A THESIS

Submitted in partial fulfilment of the
requirements for the award of the degree
of
Master of Science

by

Palzor Lepcha

DISCIPLINE OF PHYSICS
INDIAN INSTITUTE OF TECHNOLOGY, INDORE
June, 2023

INDIAN INSTITUTE OF TECHNOLOGY INDORE

CANDIDATE'S DECLARATION

I hereby certify that the work which is being presented in the thesis entitled **Magnetic Fabry-Perot Interferometer For Valley Filtering In Silicene** in the partial fulfillment of the requirements for the award of the degree of **Master of Science** and submitted in the **Department of Physics, Indian Institute of Technology Indore**, is an authentic record of my work carried out during the period from July 2022 to June 2023 under the supervision of **Dr. Alestin Mawrie, Asst. Professor, Indian Institute of Technology Indore.**

The matter presented in this thesis has not been submitted by me for the award of any other degree of this or any institute.

Palzor Lepcha 07/06/2023

Signature of the student with date

(Palzor Lepcha)

This is to certify that the above statement made by the candidate is correct to the best of my knowledge.

Signature of the Supervisor of M.Sc. thesis (with date)

(Dr. Alestin Mawrie) Mawrie 07/06/2023

Palzor Lepcha has successfully given his M.Sc. Oral Examination held on 6th **June, 2023**

Signature of Supervisor of M.Sc. thesis — Convener, DPGC

Date: Mawrie 07/06/2023 — Date: 7/6/2023

Signature of PSPC Member no. 1 — Signature of PSPC Member no. 2

Date: June 7, 2023 — Date: 07/06/2023

ACKNOWLEDGEMENTS

I would like to take this opportunity to express my sincere gratitude to everyone who has contributed to the successful completion of my thesis.

First and foremost, I would like to thank my thesis supervisor ***Dr. Alestin Mawrie****, for their guidance, support, and encouragement throughout my project research and let me work in* ***Quantum Transport Group****. Their expertise and insights have been invaluable in shaping my work and ensuring its quality.*

I would also like to express my gratitude to the PSPC members of my project thesis committee, ***Prof. Somaditya Sen*** *and* ***Prof. Sudeshna Chattopadhyay****, for their insightful feedback and suggestions. Their constructive criticism has helped me improve my work and develop my project research skills.*

I am also deeply grateful to my family and friends, for their unwavering support and encouragement. Their love and encouragement have been a constant source of strength and inspiration throughout this journey.
Additionally, I would like to thank all the participants who generously gave their time and shared their experiences with me. Without their cooperation, this project would not have been possible. Special thanks to Miss Shusmita Shah research scholar, Tarun Indoriya , Laksha Pradip Das, Hitesh Arora, Vikash, Joginder, Kumar Saumya, and Quantum Transport Group.

Finally, I would like to extend my gratitude to the staff and faculty of the Indian Institute Of Technology, Indore, for providing me with the resources and opportunities that have helped me to grow and develop as a master's student. Thank you all for your invaluable contributions to my project thesis.

Palzor Lepcha

ABSTRACT

Graphene and silicene share several fundamental properties due to their similar honeycomb lattice structures. However, the replacement of carbon atoms with silicon atoms introduces unique characteristics in silicene. Silicene exhibits a buckled structure with alternating out-of-plane displacements, significantly influencing its electronic, mechanical, and thermal properties. Unlike graphene, silicene possesses a bandgap, rendering it potentially useful for electronic and optoelectronic applications. In this thesis, we start with the Dirac nature of quasi-particle in graphene and Silicene and the behavior of Landau levels in the presence of magnetic fields. In the case of graphene, the absence of a band gap allows low-energy electrons near the K and K' points to propagate over long distances without scattering. This is a consequence of the linear dispersion relation and the absence of any energy barriers for electron transmission. As a result, electrons can exhibit high electron mobility. Silicene has the advantage of non-degenerate valleys (K and K' states) and also possesses a band gap as a result of the intrinsic spin-orbit coupling. In this thesis, we propose a quantum Fabry Perot geometry that filters out these non-degenerate valley states.

Contents

List of Figures

Chapter 1

Magnetic Fabry-Perot Interferometer For Valley Filtering In Graphene

For understanding purposes, we start with a tight binding result that describes graphene before we analyse the behaviour of silicone .

Graphene is a single-layer arrangement of carbon atoms to form a hexagonal lattice[1]. Graphene and Silicene have various fundamental properties in common due to their similar honeycomb lattice structures. However, replacing carbon atoms with silicon atoms introduces unique characteristics in Silicene. A buckled structure in Silicene introduces intrinsic properties such as spin-orbit coupling and an intrinsic Zeeman-like splitting.

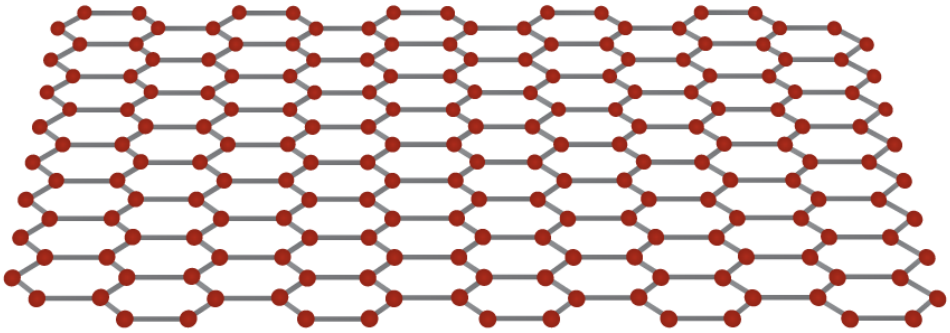

Figure 1.1: Structural representation of Graphene monolayer.

1.1 Tight-Binding Hamiltonian

The figure below shows the lattice vectors and the first Brillouin zone of graphene. The vectors are defined as

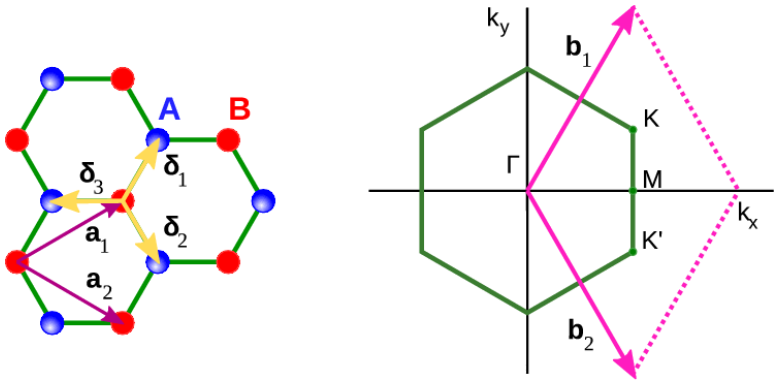

Figure 1.2: Honeycomb structure of Graphene and its Brillouin zone with two inequivalent Dirac points K,K'

$$a_1 = \frac{a}{2}(3, \sqrt{2})$$

$$a_2 = \frac{a}{2}(3, -\sqrt{3})$$

$$\delta_1 = \frac{a}{2}(1, \sqrt{3})$$

$$\delta_2 = \frac{a}{2}(1, -\sqrt{3})$$

$$\delta_3 = -a(1, 0)$$

The vector associated with the Dirac points are as follows

$$K = \frac{2\pi}{3\sqrt{3}a}(\sqrt{3}, 1)$$

$$K' = \frac{2\pi}{3\sqrt{3}a}(\sqrt{3}, -1)$$

The simplest tight-binding Hamiltonian for graphene can be written as[2]

$$\hat{H} = -t \sum_{ij} (\hat{a}_i \hat{b}_j + \hat{b}_j^{\dagger} \hat{a}_i)$$

Having known the lattice vectors and the tight-binding Hamiltonian, it is easy to compute the dispersion relation in graphene. into account the spe-

cific geometry and symmetries of graphene, the tight-binding Hamiltonian can be diagonalized to obtain the energy spectrum and wavefunctions of the system. The dispersion relation obtained using tight binding approach exhibits two inequivalent Dirac points at the corners of the Brillouin zone, known as the K and K' points[3][4]. These points give rise to the linear energy-momentum dispersion characteristic of massless Dirac fermions.

When atoms are placed onto the graphene hexagonal lattice, the overlap among the $p_z(\pi)$ orbitals with s, p_x, and p_y orbitals are zero by symmetry. So, the p_z electrons forming the π bands in graphene can be treated independently. Within this π-band approximation, using a conventional tight-binding model, the dispersion relation (restricted to first-nearest-neighbor interactions only) produces energy of the electrons with wave vector[5].

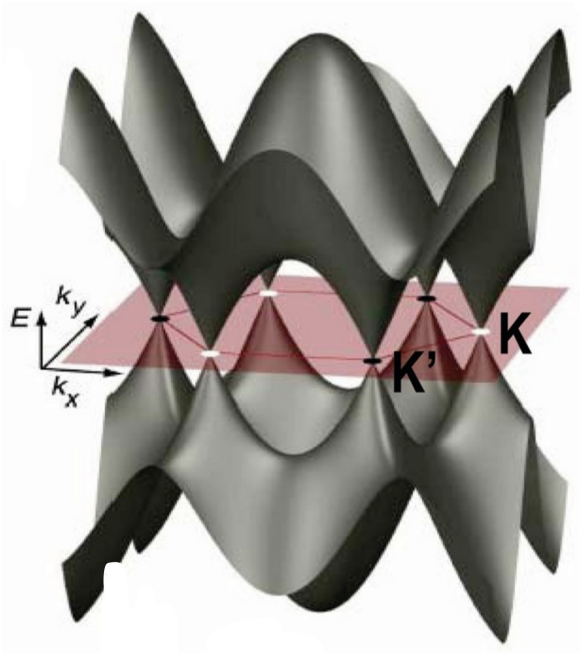

Figure 1.3: Band Structure Of Graphene over the whole Brillouin zone.

$$E(k) = \pm \mid t \mid \sqrt{3 + 2Cos(\sqrt{3}k_x a) + 4Cos(\frac{\sqrt{3}}{2}k_x a)Cos(\frac{3}{2}k_y a)}$$

where E(k) is the energy of the charge carrier with momentum k, "t" is hoping amplitude and "a" is lattice constant (2.46 Å) and k_x/k_y are the momentum in x/y-directions respectively. and v_F is the Fermi velocity.

Also, +/- sign indicates the two possible directions of the momentum vector relative to the K/K' points. The dispersion is shown in Fig. [1.3]. Valence and conduction bands meet at the six vertices of the hexagonal Brillouin zone and form linearly dispersing Dirac cones. This linear dispersion leads to several unique electronic properties such as the absence of backscattering and the existence of a minimum conductivity due to the Dirac cone crossing at the Fermi level. These properties make graphene a promising material for various electronics, photonics, and energy conversion applications [6].

1.2 Landau Level

In this part, Landau Level is introduced to exploit more about the energy level physics. The Landau level is a term used to describe the quantization of electronic energy levels in a magnetic field. It arises due to the interaction between charged particles and a magnetic field which enforce the particles to move in a circular orbits around the magnetic field lines.

The Landau level energy levels are discrete and equidistant, and they are determined by the strength of the magnetic field, the charge of the particle, and its mass. In the presence of a magnetic field, the electronic energy levels become quantized into Landau levels, which can be described as a set of harmonic oscillator states. The Landau levels are characterized by their quantum number, which is related to the number of flux quanta that penetrate the area enclosed by the orbit of the charged particle. The energy of the Landau level increases with the quantum number, and the spacing between adjacent Landau levels is proportional to the strength of the magnetic field. The Landau levels have been observed in a variety of systems, including two-dimensional electron gases, semiconductors, and metals. In some materials, such as graphene, the Landau levels have unique properties due to its charge carriers' peculiar energy-momentum dispersion relation, which can lead to the appearance of chiral edge states and the quantum Hall effect.

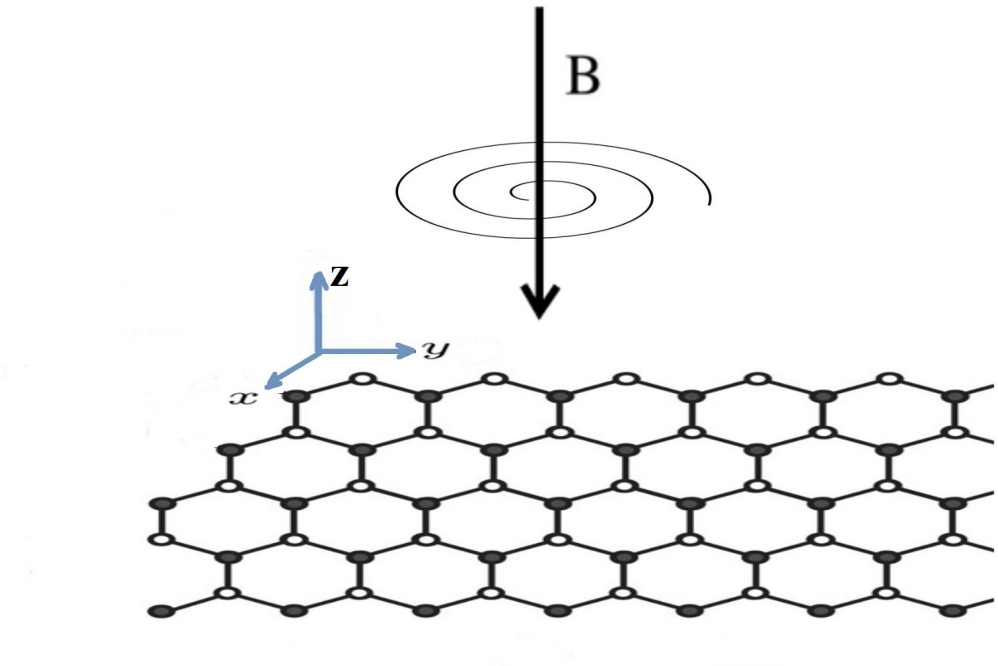

Figure 1.4: A schematic representation of normally incident magnetic field (**B**) on Graphene-monolayer .

1.3 Landau Level In Graphene And The Edge Effect

In graphene, a two-dimensional material made up of carbon atoms arranged in a hexagonal lattice, the Landau levels describe the quantization of electronic states in a magnetic field. The Landau levels in graphene are particularly interesting due to its charge carriers' peculiar energy-momentum dispersion relation (electrons and holes).

The edge states in graphene arise due to the breaking of the translational symmetry at the edges of the material, which leads to the confinement of the electronic states. In the presence of an external magnetic field, the edge states in graphene can give rise to a quantized Hall conductance, which is a hallmark of the quantum Hall effect. The edge states in graphene can be described by a one-dimensional Dirac-like equation, which

is a simplified version of the two-dimensional Dirac equation that describes the bulk electronic states in graphene. This one-dimensional Dirac equation takes into account the edge potential and the magnetic field and gives rise to chiral edge modes that propagate along the edges of the material. The chiral edge modes in graphene have a unique dispersion relation that is linear in energy and momentum, similar to the bulk electronic states in graphene. However, unlike the bulk states, the chiral edge modes only propagate in one direction along the edge and are completely immune to backscattering, which means that they can propagate without any dissipation or loss of energy. The chiral edge modes in graphene have a unique dispersion relation that is linear in energy and momentum, similar to the bulk electronic states in graphene. However, unlike the bulk states, the chiral edge modes only propagate in one direction along the edge and are completely immune to backscattering, which means that they can propagate without any dissipation or loss of energy.

1.4 Landau Level Of Graphene

First, we placed Graphene in a magnetic field perpendicular to the (x, y) plane and we observed electrons near Fermi energy which are described by the Dirac electron near K and K$'$ points. We choose the Landau gauge $\mathbf{A} = (0, A_y) = (0, xB_0)$ such that the Hamiltonian in the momentum space at one of the valley points reads[7][8]

$$H = \hbar v_f(\sigma_x P_x + \sigma_y(P_y + eA_y)) \tag{1.1}$$

where P_x and P_y are momentum in x and y direction respectively and $\sigma_{x,y}$ are Pauli matrices and Fermi velocity $v_f = 8 \times 10^5$m/s. Now the Hamiltonian is structured as

$$H = \begin{pmatrix} 0 & P_x - i(eA_y - P_y)\hbar v_f \\ P_x + i(eA_y - P_y)\hbar v_f & 0 \end{pmatrix} \tag{1.2}$$

From the above expression, we can say that momentum along y-directions commutes with the system Hamiltonian as $[H, P_y] = 0$. In terms of the ladder operators a and $a^\dagger$

$$P_x = \frac{i}{\sqrt{2}l_B}(a^\dagger - a) \tag{1.3}$$

$$P_y = \frac{-\sqrt{2}}{l_B}(a^\dagger + a) \tag{1.4}$$

where $l_B = \frac{c}{eB_0}$. Where $a^\dagger$ and a are raising and lowering operators defined as $a^\dagger|n\rangle = \sqrt{n+1}|n+1\rangle$ and $a|n\rangle = \sqrt{n}|n-1\rangle$. Using the above relation Hamiltonian reduces to

$$H = \hbar\frac{\sqrt{2}}{l_B}v_f \begin{pmatrix} 0 & ia^\dagger \\ ia & 0 \end{pmatrix} \tag{1.5}$$

Now putting the above equations in Schrodinger equation $H\psi = E\psi$;

$$\begin{pmatrix} 0 & ia^\dagger \\ ia & 0 \end{pmatrix} \begin{pmatrix} A_n\phi_n(\frac{x+\frac{\hbar k_y}{eB_0}}{l_c}) \\ B_n\phi_{n-1}(\frac{x+\frac{\hbar k_y}{eB_0}}{l_c}) \end{pmatrix} = \tilde{E_n}' \begin{pmatrix} A_n\phi_n(\frac{x+\frac{\hbar k_y}{eB_0}}{l_c}) \\ B_n\phi_{n-1}(\frac{x+\frac{\hbar k_y}{eB_0}}{l_c}) \end{pmatrix}$$

$$\tilde{E_n'} = \frac{E_n}{\hbar\frac{\sqrt{2}}{l_B}v_f}$$

$$\begin{pmatrix} iB_n\sqrt{n+1}\phi_n(\frac{x+\frac{\hbar k_y}{eB_0}}{l_c}) \\ -iA_n\phi_{n-1}(\frac{x+\frac{\hbar k_y}{eB_0}}{l_c}) \end{pmatrix} = \tilde{E_n}' \begin{pmatrix} A_n \\ B_n \end{pmatrix}$$

using $\mid A_n \mid^2 + \mid B_n \mid^2 = 1$ gets the two equation :

$$iB_n\sqrt{n+1}\phi_n = \tilde{E}'A_n; \tag{1.6}$$

$$-iA_n\sqrt{n+1}\phi_{n-1} = \tilde{E}'B_n; \tag{1.7}$$

Now taking the determinant and solving further we get the Landau level as:

$$E_n = \pm\sqrt{2n}\hbar\omega_c; \tag{1.8}$$

The $\pm$ signs indicate the valley index, which is related to the two inequivalent valleys (K and K') in the graphene Brillouin zone. $\omega_c = \frac{eB}{mc}$ is the cyclotron frequency, where e is the elementary charge, B is the magnitude of the perpendicular magnetic field, m is the electron mass, and c is the speed of light.

From the above expression, we can make the following observations: Effective band velocity along the transport directions seems to be equal to zero;

$$v_y = \frac{dE_n}{dk_y} = 0$$

The Landau levels in graphene are highly degenerate. For each value of n, there are fourfold degenerate states, corresponding to the two valleys and two spin orientations of the electrons. The Landau level spectrum is symmetric concerning $n = 0$, which means that there are no energy differences between positive and negative values of n. This is a consequence of the particle-hole symmetry of the graphene Dirac spectrum. The edge effect has not been taken into consideration.

To counter the above problem we introduce a special function called parabolic cylindrical functions. The energy levels obtained from the parabolic cylindrical functions can then be used to calculate various transport properties, such as conductance, transmission probabilities, or current-voltage characteristics of the system. The behavior of electrons in the presence of external magnetic fields or interactions with other particles can also be analyzed using these functions. Furthermore, parabolic cylindrical functions can be used in the analysis of scattering processes in cylindrical geometries. By considering the incident and scattered wavefunctions, one can express the scattering coefficients or transmission probabilities in terms of the parabolic cylindrical functions, providing insights into the scattering behavior of quantum particles in the system.

1.5 Edge State

Now considering electron-like scattering entering from the left side, with incoming momentum $p = (P_x, P_y)$.Therefore scattering states in regions I and III are given by

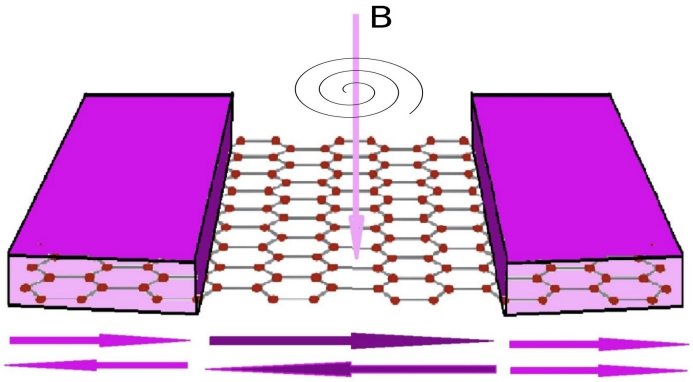

Figure 1.5: Schematic diagram of Edge State Effect where region II is exposed in magnetic fields.

$$\psi_I(x) = \begin{pmatrix} 1 \\ e^{i\phi} \end{pmatrix} e^{iP_x x} \pm r \begin{pmatrix} 1 \\ -e^{-i\phi} \end{pmatrix} e^{-iP_x x} \tag{1.9}$$

$$\psi_{II}(x) = \sum_{\pm} c_{\pm} \begin{pmatrix} D_{\mu-1}[\pm\sqrt{2}(\frac{x}{l_B} + P_y l_B)] \\ \pm i\frac{\sqrt{2}}{\epsilon l_B} D_{\mu}[\pm[\sqrt{2}(\frac{x}{l_B} + P_y l_B)] \end{pmatrix} \tag{1.10}$$

And,

$$\psi_{III}(x) = t\sqrt{\frac{P_x}{P'_x}} \begin{pmatrix} 1 \\ e^{i\phi'} \end{pmatrix} e^{iP_x x} \tag{1.11}$$

Where D_μ[9] is a parabolic cylindrical of degree n. The parabolic cylindrical functions describe the spatial distribution of the electron wavefunction in the direction perpendicular to the graphene plane. They have a Gaussian-like envelope that becomes more tightly confined to the graphene plane as the Landau level index increases. The valley index s determines the sign of the wavefunction in each of the two valleys, which are related by time-reversal symmetry.

1.6 Transmission Coefficients Across The Magnetic Barrier

In the presence of a perpendicular magnetic field, the electronic states in graphene are quantized into Landau levels, each of which is characterized by a discrete energy spectrum. When a graphene sheet is subjected to a magnetic barrier, the Landau levels are affected by the barrier potential, which can lead to interesting quantum transport phenomena. To calculate the transmission probability, we need to introduce the probability current[10][11];

$$J_x = v_f Re[\psi_B^*(cos\phi\psi_A + sin\phi_{c)}]$$

$$J_y = v_f[\psi_B^*](cos\phi\psi_A - sin\phi\psi_c)]$$

Therefore using the boundary conditions, we can calculate the coefficients.

$$\psi_I(x)|_{-d} = \psi_{II}(x)|_{-d} \tag{1.12}$$

$d = L/2$

$$\psi_{II}(x)|_d = \psi_{III}(x)|_d \tag{1.13}$$

Therefore from above boundary condations, we can describe the wave function as follows;

$$\psi_I(-d) = \begin{pmatrix} 1 \\ e^{i\phi} \end{pmatrix} e^{iP_x d} + r \begin{pmatrix} 1 \\ -e^{-i\phi} \end{pmatrix} e^{-iP_x d}; \tag{1.14}$$

$$\psi_{II}(-d) = a \begin{pmatrix} y_1^+ \\ i\frac{\sqrt{2}}{\epsilon l_B} z_1^+ \end{pmatrix} + b \begin{pmatrix} y_1^- \\ -i\frac{\sqrt{2}}{\epsilon l_B} z_1^- \end{pmatrix}; \tag{1.15}$$

$$\psi_{II}(d) = a \begin{pmatrix} y_1^+ \\ i\frac{\sqrt{2}}{\epsilon l_B} z_1^+ \end{pmatrix} + b \begin{pmatrix} y_1^- \\ -i\frac{\sqrt{2}}{\epsilon l_B} z_1^- \end{pmatrix}; \tag{1.16}$$

$$\psi_{III}(d) = t\sqrt{\frac{p_x}{p'_x}} \begin{pmatrix} 1 \\ e^{i\phi'} \end{pmatrix} e^{ip'_x d}; \tag{1.17}$$

Applying the above boundary conditions to calculate the coefficients;

$$\begin{pmatrix} 1 \\ e^{i\phi} \end{pmatrix} e^{iP_x d} + r \begin{pmatrix} 1 \\ -e^{-i\phi} \end{pmatrix} e^{-iP_x d} = a \begin{pmatrix} y_1^+ \\ i\frac{\sqrt{2}}{\epsilon l_B} z_1^+ \end{pmatrix} + b \begin{pmatrix} y_1^- \\ -\, i\frac{\sqrt{2}}{\epsilon l_B} z_1^- \end{pmatrix}$$

Also

$$t\sqrt{\frac{P_x}{P'_x}} \begin{pmatrix} 1 \\ e^{i\phi'} \end{pmatrix} e^{iP_x d} = \begin{pmatrix} y_2^+ \\ i\frac{\sqrt{2}}{\epsilon l_B} z_2^+ \end{pmatrix} + b \begin{pmatrix} y_2^- \\ -\, i\frac{\sqrt{2}}{\epsilon l_B} z_2^- \end{pmatrix}$$

Therefore, solving the above two expressions leads to four equations:

$$e^{-idp_x} + e^{idp_x} r - b y_1^- - a y_1^+ = 0;$$

$$e^{-idp_x + i\phi} - e^{idp_x - i\phi} r + \frac{i\sqrt{2} b z_1^-}{\epsilon l_B} - \frac{i\sqrt{2} a z_1^+}{\epsilon l_b} = 0;$$

$$-e^{idp'_x} \sqrt{\frac{p_x}{p'_x}} t + b y_2^- + a y_2^+ = 0;$$

$$-e^{idp'_x + i\phi} \sqrt{\frac{p_x}{p'_x}} t - \frac{i\sqrt{2} b z_2^-}{\epsilon l_B} + \frac{i\sqrt{2} a z_2^+}{\epsilon l_B} = 0;$$

Solving the above equation we get the coefficients as follows:

$$a = -\frac{(e^{-idP_x}(1 + e^{2i\phi}\epsilon l_B(i\sqrt{2} z_2^- + e^{i\phi' y_2^-}\epsilon l_B)}{\xi_a}$$

$$\text{where, } \xi_a = (2e^{i\phi} z_1^+ z_2^- - 2e^{i\phi} z_1^- z_2^+ i\sqrt{2} e^{i(\phi+\phi')} y_2^+ z_1^- \epsilon l_B$$

$$-i\sqrt{2} e^{i(\phi+\phi')} y_2^- z_2^+ \epsilon l_B - i\sqrt{2} y_1^+ z_2^- \epsilon l_B) S_p$$

$$\text{and } S_p = -i\sqrt{2} y_1^- z_2^+ \epsilon l_B - e^{i\phi'} y_1^+ y_2^- \epsilon l_B^2 + e^{i\phi'} y_1^- y_2^+ \epsilon l_B^2$$

$$b = -\frac{((e^{idP_x}(1 + e^{2i\phi}\epsilon l_B(-i\sqrt{2} z_2^+ + e^{i\phi' y_2^+}\epsilon l_B))}{\xi_b}$$

$$\text{where, } \xi_b = (-2e^{i\phi} z_1^+ z_2^- + 2e^{i\phi} z_1^- z_2^+ + i\sqrt{2} e^{i(\phi+\phi')} y_2^+ z_2^- \epsilon l_B +$$

$$i\sqrt{2} e^{i(\phi+\phi')} y_2^- z_1^+ \epsilon l_B + i\sqrt{2} y_2^+ z_2^- \epsilon l_B) N_i$$

$$\text{and } N_i = i\sqrt{2} y_1^- z_2^+ \epsilon l_B + e^{i\phi'} y_1^+ y_2^- \epsilon l_B^2 - e^{i\phi'} y_1^- y_2^+ \epsilon l_B^2$$

$$r = -\frac{((e^{-2idP_x+i\phi})\Delta\xi)}{\xi_c}$$

where, $\Delta\xi = (-2iz_1^+z_2^- + 2iz_1^-z_2^+ - \sqrt{2}e^{i\phi'}y_2^+z_1^-\epsilon l_B -$
$\sqrt{2}e^{i\phi'}y_2^-z_1^+\epsilon l_B + \sqrt{2}e^{i\phi}y_1^-z_2^+\epsilon l_B))R_i$

and, $\xi_c = (-2ie^{i\phi}z_1^+z_2^- + 2ie^{i\phi}z_1^-z_2^+ - \sqrt{2}e^{i(\phi+\phi')}y_2^+z_1^-\epsilon l_B -$
$\sqrt{2}e^{i(\phi+\phi')}y_2^-z_1^+\epsilon l_B - \sqrt{2}y_1^+z_1^-\epsilon l_B)R_e$

$$R_i = -ie^{i(\phi+\phi')}y_1^+y_2^-\epsilon l_B^2 + ie^{i(\phi+\phi')}y_1^-y_2^+\epsilon l_B^2$$

$$R_e = -\sqrt{2}y_1^-z_2^+\epsilon l_B + ie^{i\phi'}y_1^+y_2^-\epsilon l_B - ie^{i\phi'}y_1^-y_2^+\epsilon l_B$$

Therefore we get the transmission coefficient as

$$t_K = \frac{2i\epsilon l_B\sqrt{\frac{2P'_x}{P_x}}cos\phi}{e^{i(P_x+p'_x)d}D}(y_2^+z_2^- + y_2^-z_2^+) \tag{1.18}$$

$$D = (\epsilon l_B)^2e^{i(\phi'-\phi)}(y_1^+y_2^- - y_2^+y_1^-) -$$
$$2(z_1^+z_2^- - z_2^+z_1^-) + i\sqrt{2}\epsilon l_B[e^{i\phi'}(z_1^+y_2^- + y_2^+z_1^-) + e^{-i\phi}(y_1^+z_2^- + z_2^+y_1^-)]$$

The transmission coefficient obtained above is for the K point to calculate for K' point using equations (1.20) and (1.21) wave function can be describe as follows;

$$\psi_I(-d) = \begin{pmatrix} 1 \\ e^{i\phi} \end{pmatrix}e^{iP_xd} - r\begin{pmatrix} 1 \\ -e^{-i\phi} \end{pmatrix}e^{-iP_xd}; \tag{1.19}$$

$$\psi_{II}(-d) = a\begin{pmatrix} y_1^+ \\ i\frac{\sqrt{2}}{\epsilon l_B}z_1^+ \end{pmatrix} - b\begin{pmatrix} y_1^- \\ -i\frac{\sqrt{2}}{\epsilon l_B}z_1^- \end{pmatrix}; \tag{1.20}$$

$$\psi_{II}(d) = a\begin{pmatrix} y_1^+ \\ i\frac{\sqrt{2}}{\epsilon l_B}z_1^+ \end{pmatrix} - b\begin{pmatrix} y_1^- \\ -i\frac{\sqrt{2}}{\epsilon l_B}z_1^- \end{pmatrix}; \tag{1.21}$$

$$\psi_{III}(d) = t\sqrt{\frac{p_x}{p'_x}}\begin{pmatrix} 1 \\ e^{-i\phi'} \end{pmatrix}e^{ip'_xd}; \tag{1.22}$$

$$\begin{pmatrix} 1 \\ e^{i\phi} \end{pmatrix} e^{iP_x x} - r \begin{pmatrix} 1 \\ -e^{-i\phi} \end{pmatrix} e^{-iP_x x} = a \begin{pmatrix} y_1^+ \\ i\frac{\sqrt{2}}{\epsilon l_B} z_1^+ \end{pmatrix} - b \begin{pmatrix} y_1^- \\ -i\frac{\sqrt{2}}{\epsilon l_B} z_1^- \end{pmatrix} \quad (1.23)$$

Also

$$t\sqrt{\frac{P_x}{P'_x}} \begin{pmatrix} 1 \\ e^{-i\phi'} \end{pmatrix} e^{iP_x d} = \begin{pmatrix} y_2^+ \\ i\frac{\sqrt{2}}{\epsilon l_B} z_2^+ \end{pmatrix} - b \begin{pmatrix} y_2^- \\ -i\frac{\sqrt{2}}{\epsilon l_B} z_2^- \end{pmatrix} \quad (1.24)$$

Therefore solving above equations (1.23) and (1.24) we get four equation as follows;

$$e^{-idp_x} - e^{idp_x} r - b y_1^- - a y_1^+ = 0; \quad (1.25)$$

$$e^{idp_x + i\phi} + e^{idp_x - i\phi} r + \frac{i\sqrt{2} b z_1^-}{\epsilon l_B} - \frac{i\sqrt{2} a z_1^+}{\epsilon l_B} = 0; \quad (1.26)$$

$$-e^{idp'_x} \sqrt{\frac{p_x}{p'_x}} t - b y_2^- + a y_2^+ = 0; \quad (1.27)$$

$$-e^{idp'_x - i\phi'} \sqrt{\frac{p_x}{p'_x}} t + \frac{i\sqrt{2} b z_2^-}{\epsilon l_B} + \frac{i\sqrt{2} a z_2^+}{\epsilon l_B} = 0; \quad (1.28)$$

This result in transmission coefficients for K' point is given below;

$$t_{K'} = \frac{\sqrt{\frac{2p'_x}{p_x}} e^{-id(p_x + p'_x)} (1 + e^{2i\phi})(y_2^+ z_2^- + y_2^- z_2^+) \epsilon l_B}{-i(y_1^+ y_2^- + y_1^- y_2^+) \epsilon l_B^2}; \quad (1.29)$$

$$D_1 = (2ie^{i(\phi+\phi')}(z_1^+ z_2^- + z_1^- z_2^+ + \sqrt{2}(e^{i\phi}(-y_2^+ z_1^- + y_2^- z_1^+) + e^{i\phi'}(y_1^+ z_2^- - y_1^- z_2^+)) \epsilon l_B); \quad (1.30)$$

using shorthand notation

$$y_1^{\pm} = D_{(\epsilon l_B)^2/2 - 1}[\pm\sqrt{2}(-d/l_B + P_y l_B)] \quad (1.31)$$

$$z_1^{\pm} = D_{(\epsilon l_B)^2/2}[\pm\sqrt{2}(-d/l_B + P_y l_B)] \quad (1.32)$$

Now transmission probability in the function of ϕ and ϵ for K and the K' given by;

$$T_K(\epsilon, \phi) = t_K^* . t_K \quad (1.33)$$

$$T_{K'}(\epsilon, \phi) = t_{K'}^* . t_{K'} \quad (1.34)$$

The above polar plot is the transmission probability vs incident angle

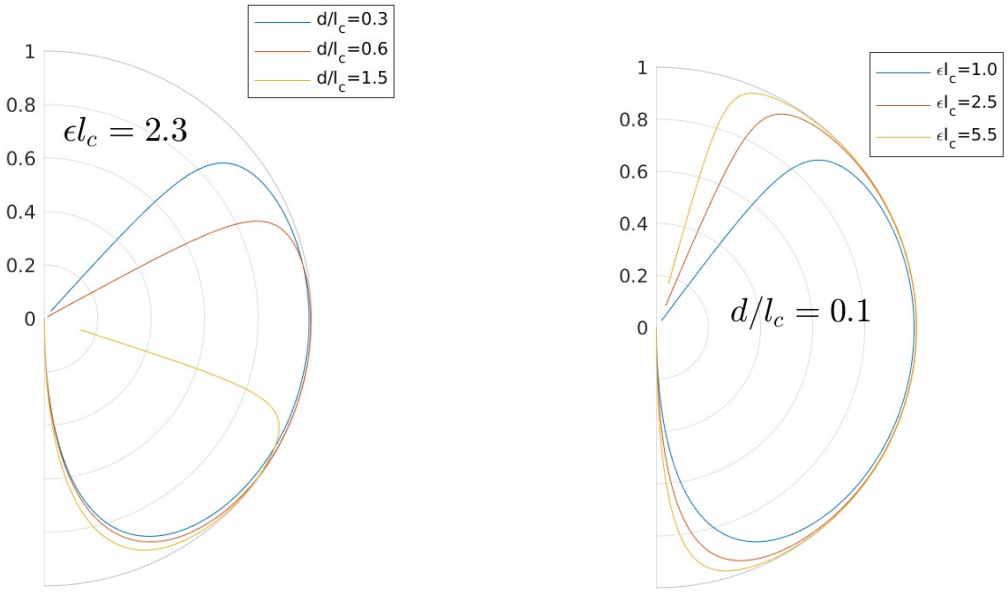

Figure 1.6: Polar plots depicting the transmission probability $T(\phi)$ as a function of magnetic barrier width 2d and energy ϵ. a) T is a function of barrier width at fixed energy $\epsilon l_c = 2.3$. b) T is a function of ϵ keeping $d/l_c = 0.1$.

at various energy ϵ. Where figure (a) plots at K points at fixed energy $\epsilon l_c = 0.1$.Where and figure (b) plots for K' point at fixed energy $\epsilon l_c = 0.1$. Where the blue line is at 1, orange at 2.5, and yellow at 5.5. where we are striking some energy to the magnetic barrier the energy gets taking the circular loop due to the cyclotron energy as shown above. The shape of the transmission probability vs. energy plot depends on the specific properties of the barrier or interface and the incident particle. Factors such as the height and width of the barrier, the potential profile, and the characteristics of the incident particle (e.g., mass, charge) influence the overall behavior of the transmission probability.

Chapter 2

Magnetic Fabry-Perot Valley Interferometer Filtering In Silicene

Silicene is a two-dimensional material composed of a single layer of silicon atoms arranged in a honeycomb lattice, similar to graphene. However, silicene is less well-known and less well-studied than graphene. Silicene has some properties similar to graphenes, such as high conductivity and high mechanical strength, but it also has some unique properties that make it potentially useful for certain applications[12]. For example, silicene is a semiconductor, which means that it can be used in electronic devices such as transistors. It also has a strong interaction with light, which makes it a promising material for optoelectronic applications. The band gap of silicene can be modulated by applying a perpendicular electric field, thus inducing a topological phase transition as the electric field increases[13][14]. However, silicene is more difficult to produce and work with than graphene. Unlike graphene, which can be easily obtained by peeling layers from graphite, silicene must be grown on a substrate. Additionally, the properties of silicene can be strongly influenced by the substrate it is grown on and the conditions used during growth.

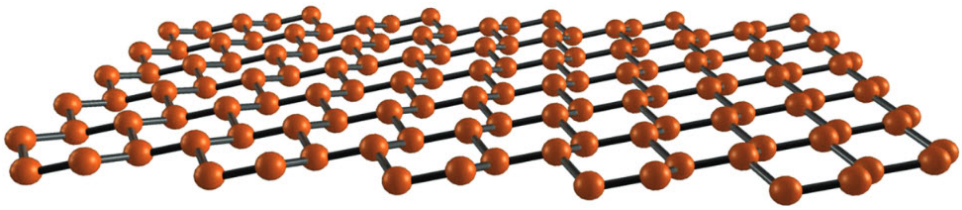

Figure 2.1: Structure of Silicene.

2.1 Why Silicene?

Silicene and graphene are both two-dimensional materials that have generated a lot of interest in recent years due to their unique electronic, mechanical, and optical properties. Silicene is a single layer of silicon atoms arranged in a honeycomb lattice, similar to graphene which is a single layer of carbon atoms arranged in a similar lattice. Compared to graphene, silicene has a stronger interaction with substrates due to the presence of heavier silicon atoms, which can lead to enhanced stability and improved electronic properties. However, the synthesis and manipulation of silicene is more challenging than graphene due to the reactivity of silicon and the lack of a suitable substrate to support its growth. On the other hand, graphene has excellent electronic conductivity and mechanical strength, and its production has been well-established. It has been used in various applications such as electronics, energy storage, and even biomedical devices. In summary, both silicene and graphene have unique properties that make them suitable for different applications. While silicene may offer improved stability and electronic properties, graphene has more established synthesis techniques and a wider range of applications.

2.2 Valley Degeneracy Lifting

The valley splitting in silicene can be characterized by measuring the energy difference between the K and K' valleys at the Dirac point, where the valence and conduction bands intersect. This splitting occurs due to the interaction between the spin and orbital degrees of freedom of electrons, which arises from the strong spin-orbit coupling present in

silicene. Unlike graphene, silicene exhibits a stronger spin-orbit coupling due to the heavier nature of silicon compared to carbon. The spin-orbit coupling in silicene arises from the interaction between the electrons and the electric field generated by the atomic nuclei. This coupling leads to the lifting of the degeneracy between the K and K' valleys, resulting in distinct energy levels for each valley. This phenomenon has significant implications for the electronic and transport properties of silicene.

One consequence of the valley splitting is the formation of a band gap at the Dirac point, which is absent in pristine graphene. The size of this band gap can be manipulated by external factors such as electric fields, strain, and doping, offering opportunities for tuning the electronic properties of silicene. This tunability makes silicene a promising material for various applications including field-effect transistors, spintronics, and optoelectronics.

2.3 Dispersion Relation In Silicene

The dispersion relation in silicene characterizes the relationship between the energy and momentum of electrons traversing the material. It provides insights into the behavior of electrons under the influence of external forces, such as electric or magnetic fields. Unlike graphene, the dispersion relation in silicene exhibits distinct characteristics due to the presence of a small energy gap at the Dirac points.

In graphene, the energy bands at the Dirac points intersect, resulting in a linear dispersion relation where the energy varies linearly with the momentum. However, in silicene, there exists a small energy gap between the valence and conduction bands at the Dirac points. This energy gap introduces a modification to the dispersion relation, causing it to be parabolic in nature near the Dirac points. As a consequence, the behavior of electrons in silicene near these points differs from that in graphene due to the presence of this energy gap.

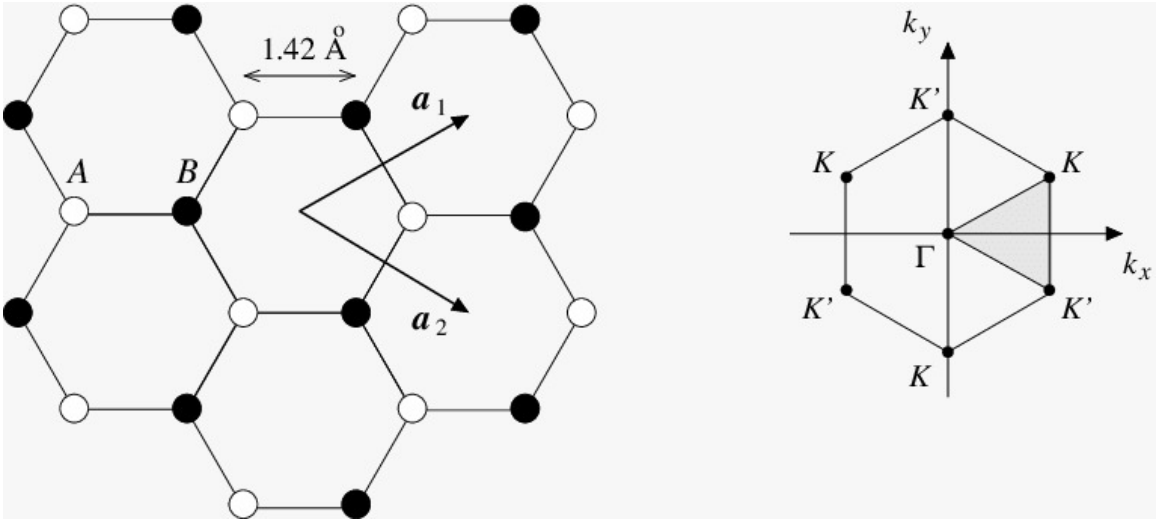

Figure 2.2: Honeycomb Structure Of Silicene and its Brillouin zone with two inequivalent Dirac points K,K'.

The Hamiltonian in graphene is given by

$$H = \hbar v_f(k_x\sigma_x - \eta(k_y + eA_y)\sigma_y) + \Delta\eta\sigma\sigma_z \tag{2.1}$$

The dispersion relation in silicene can be described by the following equation:

$$E(k) = \pm\sqrt{(\Delta_z - \Delta_{so}\eta\sigma)^2 + k^2v_f^2\hbar^2}$$

where E(k) is the energy of an electron with momentum k, t is the hopping parameter between neighboring silicon atoms, a is the lattice constant of silicene, and the $\pm$ sign indicates the presence of two bands with opposite spin. The energy gap at the Dirac points in silicene can be tuned by applying an external electric field or by doping the material with other atoms. This property makes silicene a potentially useful material for electronic applications, such as field-effect transistors and other nanoelectronic devices.

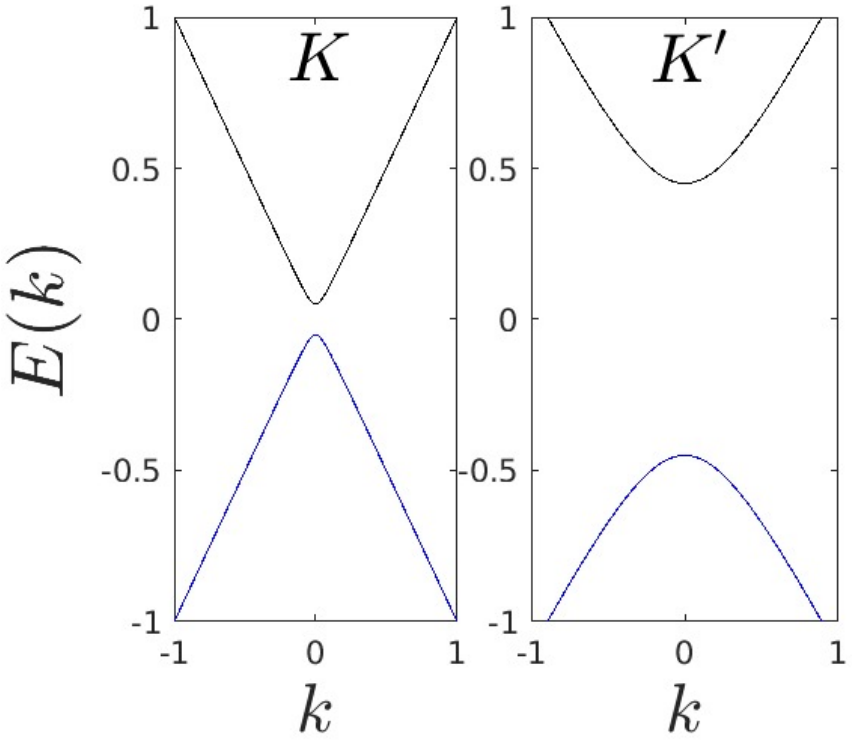

Figure 2.3: Energy Band Dispersion at K and the K' points.

The presence of the band gap introduces an energy barrier for electron transmission. Electrons with energies near the K and K' points need to overcome this barrier to propagate. The transmission efficiency depends on the band gap size. The presence of scattering mechanisms, such as defects or impurities, can also affect electron transmission at the K and K' points in silicene. Considering the above energy band gap we are going to filter out the valley degeneracy in silicene using a magnetic fabry-perot interferometer.

2.4 Magnetic Fabry-Perot Interferometer

The Fabry-Perot interferometer is a classical optical device that consists of two partially reflecting mirrors separated by a fixed distance[15]. It is commonly used to study interference phenomena in optics. However, in the context of quantum transport, the Fabry-Perot interferometer can be extended to study the behavior of quantum particles, such as electrons or

photons, as they propagate through a physical system. In a typical setup, the Fabry-Perot interferometer in quantum transport consists of a central region, often referred to as the quantum dot or cavity, which is coupled to two leads or reservoirs. The leads act as a source and drain for the transport of quantum particles. When a particle, such as an electron, is injected into the interferometer from the source lead, it can propagate through the quantum dot and exit through the drain lead. The interference of the particle waves is then observed at the drain lead. The interference pattern depends on various factors, including the energy levels of the quantum dot, the energy of the injected particle, and the phase accumulated by the particle during its propagation. The Fabry-Perot interferometer in quantum transport has been studied extensively in both theoretical and experimental research. It has applications in areas such as quantum computing, quantum information processing, and the investigation of fundamental quantum phenomena. The behavior of quantum particles in Fabry-Perot interferometers has also been utilized to probe the effects of electron-electron interactions, magnetic fields, and other external influences on quantum transport.

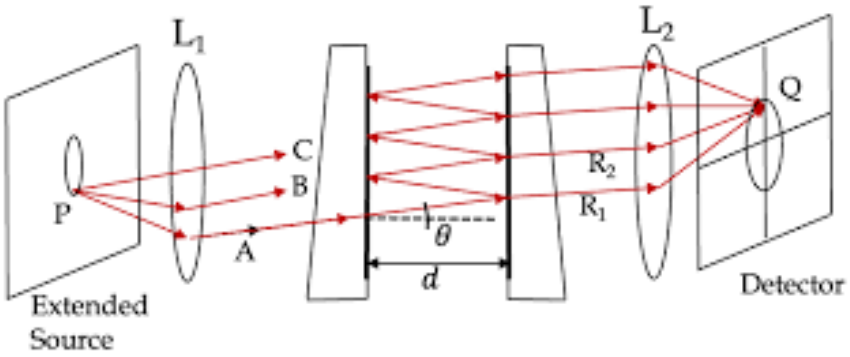

Figure 2.4: A schematic representation of Fabry-Perot setup.

2.5 Valley Polarizations

Valley polarization is a concept that arises in certain materials with a property called "valley degeneracy." In condensed matter physics, the term "valley" refers to extrema in the energy dispersion of the electronic

bands where the energy is minimized. These valleys often exist in reciprocal space and can be described as points where the energy is at a local minimum. Valley degeneracy occurs when multiple valleys have the same energy, leading to the formation of energy bands with multiple degenerate valleys. In such materials, electrons can occupy different valleys with the same energy, giving rise to the possibility of valley polarization.

2.6 Landau Level In Silicene And Edge Effect

The Landau level in silicene refers to the quantization of electronic states that occurs when the material is subjected to a perpendicular magnetic field. In silicene, the Landau level has a different structure than in graphene due to the presence of a small energy gap at the Dirac points. This gap gives rise to a Berry curvature that can affect the Landau level spectrum.

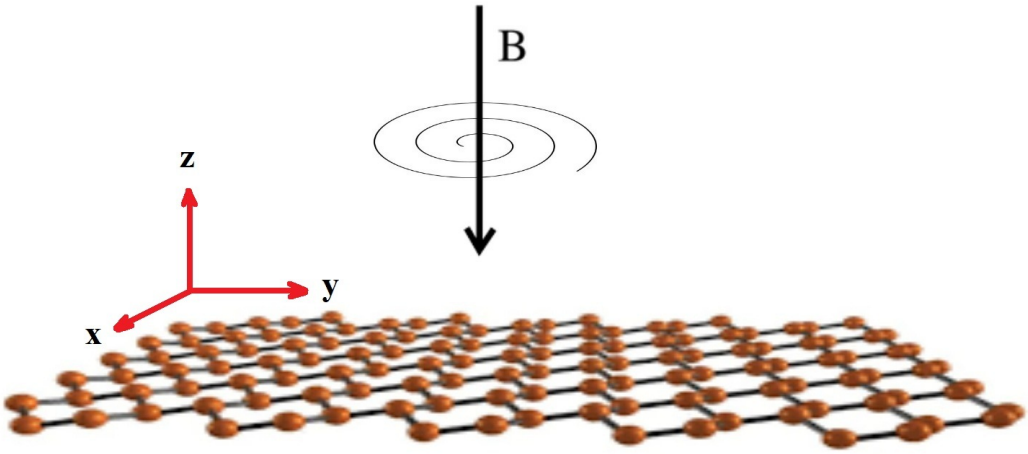

Figure 2.5: Schematic diagram of Silicene-monolayer exposed to the magnetic field in normal direction.

Edge states in silicene are electronic states that occur at the boundaries or edges of the material. They are a consequence of the topological

properties of the material, which arise from the arrangement of silicon atoms in a honeycomb lattice. In silicene, the presence of an energy gap at the Dirac points gives rise to a non-trivial topological insulating phase in the bulk of the material. This phase is characterized by the existence of edge states that propagate along the edges of the material without backscattering, even in the presence of disorder or impurities.

2.7 Landau Level In Silicene

When the Silicene is subjected perpendicular to magnetic fields, we observed electrons near Fermi energy which is described by Dirac electrons near K and K' points. Therefore Hamiltonian in momentum space reads[16]:

$$H = \hbar v_f(k_x\sigma_x - \eta(k_y + eA_y)\sigma_y) + \Delta\eta\sigma\sigma_z \tag{2.2}$$

Where $\hbar$ is reduced Plank constant,v_f is Fermi velocity,A_y comes from gauge choice which is called Landau gauge,σ_{xyz} are the Pauli matrices,η define the valley of Silicene whose value is ± 1.

$$\Delta\eta\sigma = \Delta_z - \eta\Delta_{so}\sigma \tag{2.3}$$

$$A_y = xB_0 \tag{2.4}$$

Where Δ_{so} is spin-orbit strength. Now using the above parameter and writing Hamiltonian in terms of a matrix:

$$H = \begin{pmatrix} \Delta\eta\sigma & v_f(k_x + i(eA_y + k_y)\eta)\hbar \\ v_f(k_x - i(eA_y + k_y)\eta)\hbar & -\Delta\eta\sigma \end{pmatrix} \tag{2.5}$$

From the above equation, we can clearly say that Hamaltonian concerning momentum along y direction commute which states that p_y is a good quantum number;

$$[H, p_y] = 0 \tag{2.6}$$

Where,

$$k_x = \frac{i}{\sqrt{2}l_c}(a^\dagger - a) \tag{2.7}$$

$$k_y = \frac{-\sqrt{2}}{l_c}(a^\dagger + a) \tag{2.8}$$

Substituting the above parameter Hamiltonian reduces as follows:

$$H = \hbar\frac{\sqrt{2}}{l_c}v_f \begin{pmatrix} \frac{\Delta\eta\sigma}{\hbar\frac{\sqrt{2}}{l_c}v_f} & ia^\dagger \\ -ia & \frac{-\Delta\eta\sigma}{\hbar\frac{\sqrt{2}}{l_c}v_f} \end{pmatrix} \tag{2.9}$$

Now substituting this Hamiltonian in Schrodinger equation $H\psi = E\psi$ we get:

$$\hbar\frac{\sqrt{2}}{l_c}v_f \begin{pmatrix} \frac{\Delta\eta\sigma}{\hbar\frac{\sqrt{2}}{l_c}v_f} & ia^\dagger \\ -ia & \frac{-\Delta\eta\sigma}{\hbar\frac{\sqrt{2}}{l_c}v_f} \end{pmatrix} \begin{pmatrix} A_n\phi_n(\frac{x+\frac{\hbar k_y}{eB_0}}{l_c}) \\ B_n\phi_{n-1}(\frac{x+\frac{\hbar k_y}{eB_0}}{l_c}) \end{pmatrix} = E'_n \begin{pmatrix} A_n\phi_n(\frac{x+\frac{\hbar k_y}{eB_0}}{l_c}) \\ B_n\phi_{n-1}(\frac{x+\frac{\hbar k_y}{eB_0}}{l_c}) \end{pmatrix}$$

where,

$$E'_n = \frac{E_n}{\hbar\frac{\sqrt{2}}{l_c}v_f}$$

$$\begin{pmatrix} \frac{\Delta\eta\sigma}{\hbar\frac{\sqrt{2}}{l_c}v_f}A_n\phi_n(\frac{x+\frac{\hbar k_y}{eB_0}}{l_c}) + iB_n\sqrt{n+1}\phi_n(\frac{x+\frac{\hbar k_y}{eB_0}}{l_c}) \\ -i\sqrt{n+1}A_n\phi_{n-1}(\frac{x+\frac{\hbar k_y}{eB_0}}{l_c}) - \frac{\Delta\eta\sigma}{\hbar\frac{\sqrt{2}}{l_c}v_f}B_n\phi_{n-1}(\frac{x+\frac{\hbar k_y}{eB_0}}{l_c}) \end{pmatrix} = E'_n \begin{pmatrix} A_n\phi_n(\frac{x+\frac{\hbar k_y}{eB_0}}{l_c}) \\ B_n\phi_{n-1}(\frac{x+\frac{\hbar k_y}{eB_0}}{l_c}) \end{pmatrix}$$

using $\mid A_n \mid^2 + \mid B_n \mid^2 = 1$ gets the two equation :

$$\frac{\Delta\eta\sigma}{\hbar\frac{\sqrt{2}}{l_c}v_f}A_n + iB_n\sqrt{1+n} = E'_nA_n \tag{2.10}$$

Also,

$$-i\sqrt{n+1}A_n - \frac{\Delta\eta\sigma}{\hbar\frac{\sqrt{2}}{l_c}v_f}B_n = E'_nB_n \tag{2.11}$$

Now Taking the determinant of the above two equations we get the Landau Level as :

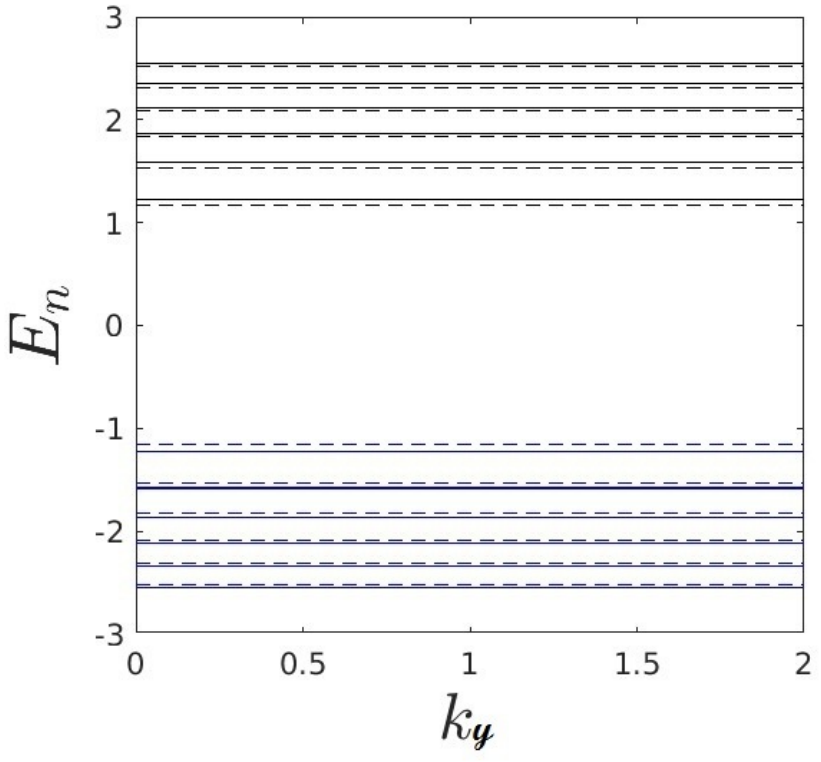

Figure 2.6: Landau levels in Silicene.

$$E_n = \pm \frac{\sqrt{\frac{l_c^2 \Delta\eta\sigma^2}{2} + (1+n)v_f^2\hbar^2}}{v_f\hbar} \tag{2.12}$$

The $\pm$ sign in the expression indicates that there are two possible energy levels at each Landau level index n. These two energy levels correspond to the spin-up and spin-down states of the electrons, which are split in energy by the Zeeman energy. The "+" sign corresponds to the energy of the spin-up state, while the "-" sign corresponds to the energy of the spin-down state.

From above we can make some observations i.e. is effective band velocity along the transport directions equal to zero.

$$v_y = \frac{dE_n}{dk_y} = 0$$

The edge effect had not been taken into consideration. So to counter the above problem we introduce a special called parabolic cylindrical function. The energy levels obtained from the parabolic cylindrical functions can

then be used to calculate various transport properties, such as conductance, transmission probabilities, or current-voltage characteristics of the system. The behavior of electrons in the presence of external magnetic fields or interactions with other particles can also be analyzed using these functions. Overall, the use of parabolic cylindrical functions in quantum transport allows for a detailed understanding of the behavior of quantum particles in cylindrical geometries. They provide a mathematical framework to describe the wavefunctions and energy levels of electrons in these systems, enabling the study of various transport properties and scattering processes relevant to quantum transport phenomena.

2.8 Egde State in the Intermediate Section

Edge states in silicene are one-dimensional electronic states that emerge at the boundaries of the material. These states are protected by topology and are robust against disorder and perturbations, making them potentially useful for various applications in electronics and spintronics.

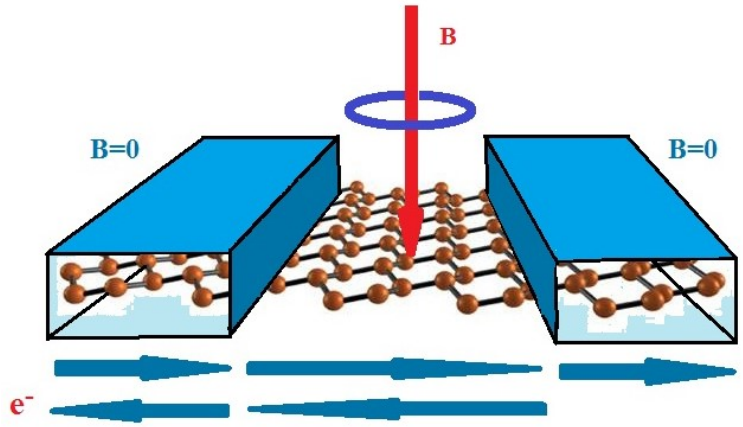

Figure 2.7: Schematic diagram of edge states where region II is exposed to a magnetic field.

$$\psi_I(x) = \begin{pmatrix} 1 \\ Pe^{i\theta} \end{pmatrix} e^{ik_x x} \pm r \begin{pmatrix} 1 \\ Pe^{-i\theta} \end{pmatrix} e^{ik_x x} \tag{2.13}$$

$$\psi_{II}(x) = \sum_{\pm} c_{\pm} \begin{pmatrix} D_{\mu-1}[\pm\sqrt{2}(\frac{x}{l_c} + k_y l_c)] \\ \pm\frac{i\sqrt{2}v_f\hbar}{l_c(\Delta_z - E + \Delta_{so})} D_{\mu}[\pm\sqrt{2}(\frac{x}{l_c} + k_y l_c)] \end{pmatrix} \tag{2.14}$$

$$\psi_{III}(x) = t \begin{pmatrix} 1 \\ Pe^{i\theta'} \end{pmatrix} e^{iq_x x} \tag{2.15}$$

Using Shorthand notations

$$\frac{v_f\hbar\sqrt{(k_x^2 + (k_y - k_\theta)^2)}}{(\Delta_z - \Delta_{so}) - \sqrt{(\Delta_z - \Delta_{so})^2 + v_f^2\hbar^2(k_x^2 + (k_y - k_\theta)^2)}} = P$$

$$\frac{\epsilon}{\tilde{\Delta}} \frac{\sqrt{(cos\theta)^2 + (sin\theta')^2}}{1 - \sqrt{1 + (\frac{\epsilon}{\tilde{\Delta}})^2((cos\theta)^2 + (sin\theta')^2)}} = P$$

$$\mu = -\frac{l_c^2(\Delta_z - E + \Delta_{so}\sigma)(\Delta_z + E + \Delta_{so}\sigma)}{2v_f^2\hbar^2}$$

$$\frac{v_f\sqrt{q_x^2 + (k_y + k_\theta)^2}\hbar}{\Delta\eta\sigma - \sqrt{\Delta\eta\sigma^2 + v_f^2\hbar^2(q_x^2 + (k_y + k_\theta)^2)}} = \frac{\epsilon}{\tilde{\Delta}} \frac{\sqrt{(cos\theta')^2 + (sin\theta)^2}}{1 - \sqrt{1 + (\frac{\epsilon}{\tilde{\Delta}})^2((cos\theta')^2 + (sin\theta)^2)}}$$

$$Q = \frac{\epsilon}{\tilde{\Delta}} \frac{\sqrt{(cos\theta')^2 + (sin\theta)^2}}{1 - \sqrt{1 + (\frac{\epsilon}{\tilde{\Delta}})^2((cos\theta')^2 + (sin\theta)^2)}}$$

In the presence of a magnetic field, the interaction between electrons and the magnetic field modifies the electronic properties of silicene. This interaction also impacts the behavior of a simple harmonic oscillator in silicene. The Lorentz force, experienced by a charged particle moving in a magnetic field, induces a force on the electrons in silicene that acts perpendicular to their direction of motion. Consequently, this force alters the oscillatory behavior of a simple harmonic oscillator in silicene, resulting in deviations from the behavior observed in the absence of a magnetic field. The effect of the magnetic field on the oscillator can be described mathematically using parabolic cylinder functions of degree n denoted as D_μ

(Gradstheyn and Ryzhik, 2014), along with complex coefficients $c_{\pm}$.

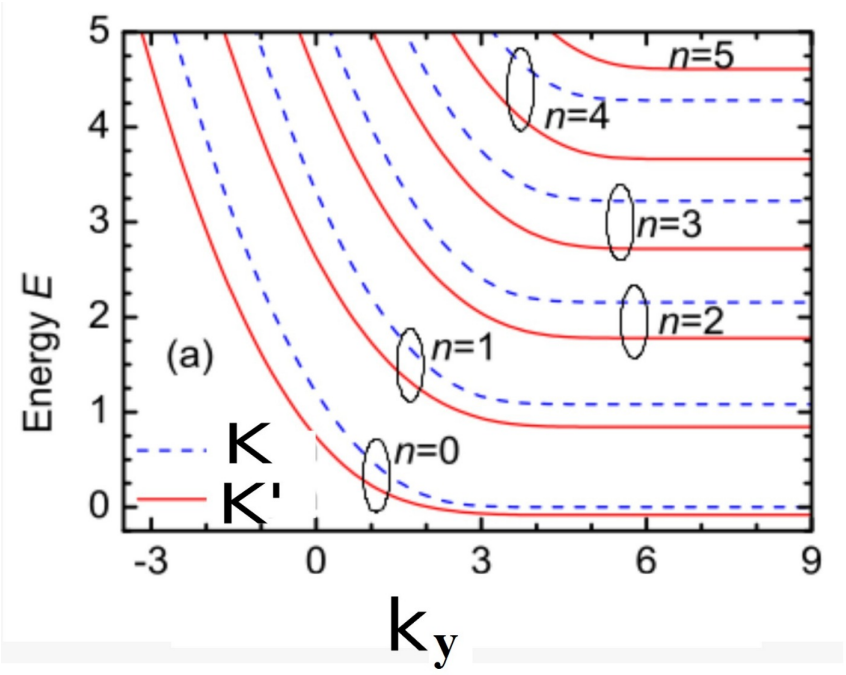

Figure 2.8: Edge states Energy spectrum.

$$v_x = \frac{dE_n}{dk_y} \neq 0;$$

When a magnetic field is applied to silicene, it can influence the motion of electrons and cause a net movement of charge carriers. This effect is similar to what occurs in graphene. The nonzero effective band velocity allows for the transport of charge carriers, making silicene a potentially interesting material for electronic and optoelectronic applications. It's worth noting that the properties of silicene can be influenced by factors such as substrate interactions and strain effects. These factors can modify the band structure and affect the effective band velocity. Therefore, the specific value of the effective band velocity in silicene would depend on the particular conditions and characteristics of the material system under consideration. In summary, when the effective band velocity along the transport direction is not zero, it indicates the presence of charge carrier movement, which is crucial for electrical conductivity in materials like semiconductors and metals. The presence of a nonzero effective band velocity can give rise to interesting transport phenomena. These phenomena can include anomalous

Hall effects, magneto-transport properties, and various quantum transport phenomena.

2.9 Tansmission Coefficients Across The Magnetic Barrier

The transmission coefficient across a magnetic barrier in silicene represents the likelihood of an electron, initially approaching the barrier from one side, being transmitted to the other side. This transmission coefficient is influenced by various factors, including the energy of the incident electron, the strength and orientation of the magnetic field, as well as the characteristics of the magnetic barrier. In order to compute the transmission probability, it is necessary to introduce the concept of probability current. The probability current is a quantity that describes the flow of probability associated with the motion of particles. In the context of electron transport, it represents the rate at which electrons cross a given point in space. By analyzing the probability current, one can gain insights into the behavior of electrons as they encounter the magnetic barrier and assess their likelihood of transmission. Calculating the transmission probability involves analyzing the probability current across the barrier region and relating it to the incident and transmitted wavefunctions of the electrons. This allows for the determination of the transmission coefficient, which quantifies the probability of electron transmission through the magnetic barrier.[10][11];

$$J_x = v_f Re[\psi_B^*(cos\phi\psi_A + sin\phi_{c)}]$$

$$J_y = v_f lm[\psi_B^*(cos\phi\psi_A - sin\phi\psi_c)]$$

Applying boundary conditions to calculate the coefficients

$$\psi_I(x)|_{-d} = \psi_{II}(x)|_{-d} \tag{2.16}$$

$d = L/2$

$$\psi_{II}(x)|_d = \psi_{III}(x)|_d \tag{2.17}$$

Therefore considering the above boundary conditions we can describe the wave function as follows;

$$\psi_I(-d) = \begin{pmatrix} 1 \\ Pe^{i\theta} \end{pmatrix} e^{-ik_x d} + r \begin{pmatrix} 1 \\ -Pe^{i\theta} e \end{pmatrix} ik_x d; \tag{2.18}$$

$$\psi_{II}(-d) = a \begin{pmatrix} y_{1'}^{+} \\ \frac{v_f i\sqrt{2}\hbar}{l_c(E+\Delta_z+\Delta_{so}\sigma)} z_1^{+} \end{pmatrix} + b \begin{pmatrix} y_{1'}^{+} \\ -\frac{v_f i\sqrt{2}\hbar}{l_c(E+\Delta_z+\Delta_{so}\sigma)} z_1^{-} \end{pmatrix}; \tag{2.19}$$

$$\psi_{II}(d) = a \begin{pmatrix} y_{1'}^{+} \\ \frac{v_f i\sqrt{2}\hbar}{l_c(E+\Delta_z+\Delta_{so}\sigma)} z_1^{+} \end{pmatrix} + b \begin{pmatrix} y_{1'}^{+} \\ -\frac{v_f i\sqrt{2}\hbar}{l_c(E+\Delta_z+\Delta_{so}\sigma)} z_1^{-} \end{pmatrix}; \tag{2.20}$$

$$\psi_{III}(d) = t \begin{pmatrix} 1 \\ Pe^{i\theta'} \end{pmatrix} e^{ip'_x d}; \tag{2.21}$$

$$\begin{pmatrix} 1 \\ Pe^{i\theta} \end{pmatrix} e^{-ik_x d} + r \begin{pmatrix} 1 \\ -Pe^{-i\theta} \end{pmatrix} e^{ik_x d} = a \begin{pmatrix} y_1^{+} \\ \frac{i\sqrt{2}v_f\hbar}{l_c(\Delta_z - E + \Delta_{so})} z_1^{+} \end{pmatrix} + b \begin{pmatrix} y_1^{-} \\ \frac{-i\sqrt{2}v_f\hbar}{l_c(\Delta_z - E + \Delta_{so})} z_1^{-} \end{pmatrix} \tag{2.22}$$

Also,

$$a \begin{pmatrix} y_1^{+} \\ \frac{i\sqrt{2}v_f\hbar}{l_c(\Delta_z - E + \Delta_{so})} z_1^{+} \end{pmatrix} + b \begin{pmatrix} y_1^{-} \\ \frac{-i\sqrt{2}v_f\hbar}{l_c(\Delta_z - E + \Delta_{so})} z_1^{-} \end{pmatrix} = t \begin{pmatrix} 1 \\ Pe^{i\theta'} \end{pmatrix} e^{iq_x d} \tag{2.23}$$

Therefore, from the above condition, four equations can be obtained :

$$e^{-idk_x} + e^{idk_x} r + b y_1^{-} - a y_1^{+} = 0; \tag{2.24}$$

$$e^{-idk_x} P e^{i\theta} - e^{idk_x} P e^{-i\theta} r - \frac{i\sqrt{2} b z_1^{-} f_f \hbar}{l_c(\Delta_z + E + \Delta_{so}\sigma)} - \frac{i\sqrt{2} a z_1^{+} f_f \hbar}{l_c(\Delta_z + E + \Delta_{so}\sigma)} = 0; \tag{2.25}$$

$$-e^{dip'_x}t + b_1 y_2^- + y_2^+ = 0; \tag{2.26}$$

$$-e^{dip'_x}Pe^{i\theta'}t - \frac{i\sqrt{2}bz_2^- v_f\hbar}{l_c(\Delta_z + E + \Delta_{so}\sigma)} + \frac{i\sqrt{2}z_2^+ v_f\hbar}{l_c(\Delta_z + E + \Delta_{so}\sigma)} = 0; \tag{2.27}$$

Solving the above equations we can obtain the transmission coefficients at K point as follows;

$$t_K = \frac{\sqrt{2}e^{-idp'_x}e^{-idk_x}l_c(1+Pe^{2i\theta})(y_1^+ z_1^- + y_1^- z_1^+)v_f(\Delta_z + E + \Delta_{so}\sigma)\hbar}{2il_c^2 Pe^{i\theta'}y_1^- y_1^+(\Delta_z + E + \Delta_{so}\sigma)^2 + F}; \tag{2.28}$$

$$F = \sqrt{2}l_c(1+Pe^{i\theta'}Pe^{i\theta})(y_1^+ z_1^- - y_1^- z_1^+)v_f(\Delta_z + E + \Delta_{so}\sigma)\hbar + 4iPe^{i\theta}z_1^- z_1^+ v_f^2\hbar^2; \tag{2.29}$$

Similarly for the K' point using equations (2.18) and (2.19) we can describe the wave functions as;

$$\psi_I(-d) = \begin{pmatrix} 1 \\ Pe^{i\theta} \end{pmatrix} e^{-ik_x d} - r \begin{pmatrix} 1 \\ -Pe^{i\theta}e \end{pmatrix} ik_x d; \tag{2.30}$$

$$\psi_{II}(-d) = a \begin{pmatrix} y_{1'}^+ \\ \frac{v_f i\sqrt{2}\hbar}{l_c(E+\Delta_z+\Delta_{so}\sigma)} z_1^+ \end{pmatrix} - b \begin{pmatrix} y_{1'}^+ \\ -\frac{v_f i\sqrt{2}\hbar}{l_c(E+\Delta_z+\Delta_{so}\sigma)} z_1^- \end{pmatrix}; \tag{2.31}$$

$$\psi_{II}(d) = a \begin{pmatrix} y_{1'}^+ \\ \frac{v_f i\sqrt{2}\hbar}{l_c(E+\Delta_z+\Delta_{so}\sigma)} z_1^+ \end{pmatrix} - b \begin{pmatrix} y_{1'}^+ \\ -\frac{v_f i\sqrt{2}\hbar}{l_c(E+\Delta_z+\Delta_{so}\sigma)} z_1^- \end{pmatrix}; \tag{2.32}$$

$$\psi_{III}(d) = t \begin{pmatrix} 1 \\ Pe^{-i\theta'} \end{pmatrix} e^{ip'_x d}; \tag{2.33}$$

Solving above equations we get four equations as follows;

$$e^{ik_x d} - e^{idk_x}r - by_1^- - ay_1^+ = 0; \tag{2.34}$$

$$e^{-ik_x d}Pe^{i\theta} + e^{idk_x}r + \frac{i\sqrt{2}bz_1^- v_f\hbar}{l_c(\Delta_z + E + \Delta_{so}\sigma)} - \frac{i\sqrt{2}az_1^+ v_f\hbar}{l_c(\Delta_z + E + \Delta_{so}\sigma)} = 0; \tag{2.35}$$

$$-e^{ip'_x d}t - by_1^- + ay_1^+ = 0; \tag{2.36}$$

$$-e^{ip'_x d}Pe^{-i\theta'}t + \frac{i\sqrt{2}bz_1^- v_f\hbar}{l_c(\Delta_z + E + \Delta_{so}\sigma)} + \frac{i\sqrt{2}az_1^+ v_f\hbar}{l_c(\Delta_z + E + \Delta_{so}\sigma)} = 0; \quad (2.37)$$

Equating the above four equations we get the transmission coefficients as;

$$T_{K'} = \frac{\sqrt{2}e^{-ip'_x d}l_c Pe^{i\theta'}(1 + Pe^{2i\theta}(y_1^+ z_1^- + y_1^- z_1^+ v_f(\Delta_z + E + \Delta_{so}\sigma)\hbar}{-2il_c^2 y_1^- y_1^+(\Delta_z + E + \Delta_{so}\sigma)^2 + F_1}; \quad (2.38)$$

$$F_1 = \sqrt{2}l_c(Pe^{i\theta'} - Pe^{i\theta})(y_1^+ z_1^- - y_1^- z_1^+)v_f(\Delta_z + E + \Delta_{so}\sigma)\hbar + 4iPe^{i\theta'}Pe^{i\theta}z_1^- z_1^+ v_f^2\hbar^2; \quad (2.39)$$

Using the shorthand notations as;

$$y_1^{\pm} = D_{(\epsilon l_c)^2/2-1}[\pm\sqrt{2}(-d/l_c + k_y l_c)]$$

$$z_1^{\pm} = D_{(\epsilon l_c)^2/2}[\pm\sqrt{2}(-d/l_c + k_y l_c)]$$

The transmission probability $T = |t|^2$ is then related to the reflection probability $R = |r|^2$ by $T + R = 1$[8].Therefore we can write the transmission probability in terms of energy ϵ and incident angle θ of K and the K' points can be written as ;

$$T_K(\epsilon, \theta) = t_K^* . t_K cos\theta'/cos\theta; \quad (2.40)$$

$$T_{K'}(\epsilon, \theta) = t_{K'}^* . t_{K'} cos\theta'/cos\theta; \quad (2.41)$$

The above polar plot is the transmission probability vs incident angle at various energy ϵ. Where the blue dotted line is for K point and the orange dotted line is for K' point. The shape of the transmission probability vs. energy plot depends on the specific properties of the barrier or interface and the incident particle. Factors such as the height and width of the barrier, the potential profile, and the characteristics of the incident particle (e.g., mass, charge) influence the overall behavior of the transmission probability.

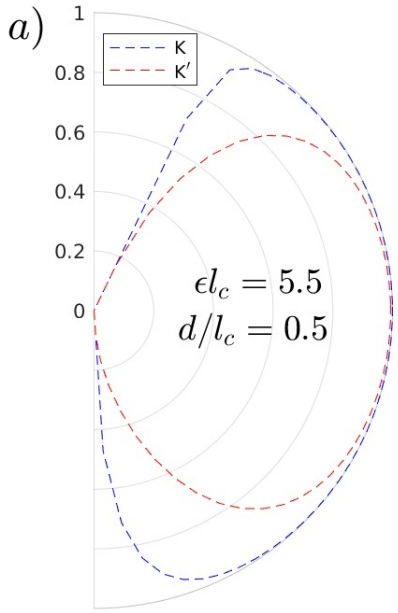

Figure 2.9: Polar graphs depicting the transmission probability $T(\theta)$ for a magnetic barrier of width $d/l_c = 0.5$ and energy $\epsilon l_c = 5.5$.

2.10 Valley Polarization

The transmission probability can be determined by considering measurable quantities, such as the total ballistic conductivity $\sigma = \sigma_+ + \sigma_-$, where the valley-dependent conductivity is obtained using the Landauer-Büttiker formula

$$\sigma_\eta = \frac{L}{W}\frac{2e^2}{\hbar}\sum_{k_y} T_\eta(k_y) \tag{2.42}$$

Here, W corresponds to the width of the barrier in the y direction, and the factor of 2 accounts for spin degeneracy. By evaluating the sum of the transmission probabilities $T_\eta(k_y)$ over the transverse wave vector k_y, the valley-dependent conductivity σ_η can be calculated[11].

To further understand the distinction between the K and K' valleys, valley polarization can be computed.[11]

$$P = \frac{\sigma_+ - \sigma_-}{\sigma_+ + \sigma_-} \tag{2.43}$$

where σ_+ and σ_- are the conductivities associated with the K and K' valleys, respectively. The valley polarization provides insight into the dif-

ferences between these two valleys in terms of their conductive properties.

$$P = \frac{\sigma_+ - \sigma_-}{\sigma_+ + \sigma_-} \tag{2.44}$$

The $\pm$ indicates the valley (K and the K' points).

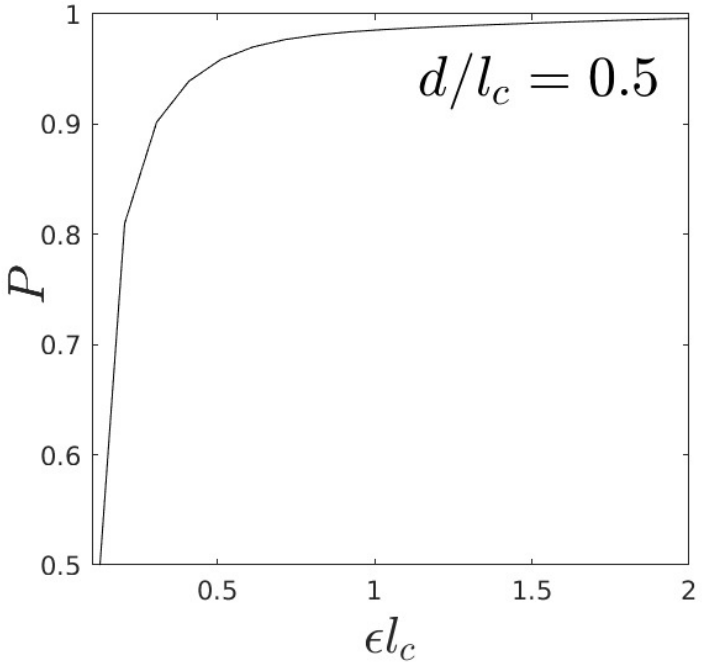

Figure 2.10: Variation in polarization as a function of the energy keeping $d/l_c = 0.5$.

The polarization values can vary from -1 to +1, where -1 indicates fully polarized electrons with a specific orientation, +1 represents fully polarized electrons with the opposite orientation, and 0 indicates no polarization or an equal distribution of charge density. The polarization of a combined electric and magnetic field as a function of energy typically fluctuates between -1 and 1 due to the nature of electromagnetic waves and the behavior of the electric and magnetic fields. The polarization of an electromagnetic wave refers to the orientation of the electric field vector as the wave propagates through space. It describes the direction in which the electric field oscillates. The polarization can be linear, circular, or elliptical, depending on the relative amplitudes and phase differences between the electric and magnetic fields. The electric field oscillates in a specific direction for a linearly polarized wave. The polarization can be horizontal,

vertical, or at any angle in between. In this case, the polarization is often described using a parameter called the polarization state, which can vary between -1 and 1. The values taken by the polarization fluctuate between -1 and 1, so $P = 1(-1)$ means that the outcoming current consists of only k(K') contribution.

Conclusion

In conclusion, graphene and silicene are two fascinating materials with unique properties that hold great potential for various applications. Graphene, a two-dimensional sheet of carbon atoms arranged in a hexagonal lattice, has exceptional mechanical, electrical, and thermal properties. It is an excellent conductor of electricity and heat, extremely strong yet flexible, and transparent. Due to degeneracy in the band structure and possessing no band bandgap, there will be weak spin-orbit coupling as a result of electron flow in the higher mobility. Graphene has been extensively studied and has found applications in diverse fields such as electronics, energy storage, sensors, and biomedical devices. However, challenges remain in terms of large-scale production, integration with existing technologies, and bandgap engineering, which limits its direct use in certain electronic applications.

Silicene, on the other hand, is a two-dimensional form of silicon, similar to graphene in structure but composed of silicon atoms. Silicene exhibits some unique properties, including a buckled honeycomb lattice structure and a tunable bandgap. It has a non-degenerate valley and also possesses a huge bandgap which also leads to the intrinsic spin coupling. Therefore we study the electron alignment in the specific band structure of silicene. Due to its bandgap tunability, it can be used in electronics, Optoelectronics energy storage, and sensors.

Both graphene and silicene have their own advantages and limitations. Graphene's extensive research and development over the years have resulted in a deeper understanding of its properties and potential applications. On the other hand, silicene is still in the early stages of exploration, and further research is required to fully harness its properties and overcome challenges related to synthesis, stability, and scalability. Graphene and silicene represent exciting areas of research and development in the field of nanomaterials.

Bibliography

[1] A. C. Neto, F. Guinea, N. M. Peres, K. S. Novoselov, and A. K. Geim, "The electronic properties of graphene," *Reviews of modern physics*, vol. 81, no. 1, p. 109, 2009.

[2] C. Bena and G. Montambaux, "Remarks on the tight-binding model of graphene," *New Journal of Physics*, vol. 11, no. 9, p. 095 003, 2009.

[3] D. F. Urban, D. Bercioux, M. Wimmer, and W. Häusler, "Barrier transmission of dirac-like pseudospin-one particles," *Physical Review B*, vol. 84, no. 11, p. 115 136, 2011.

[4] A. De Martino, A. Hütten, and R. Egger, "Landau levels, edge states, and strained magnetic waveguides in graphene monolayers with enhanced spin-orbit interaction," *Physical Review B*, vol. 84, no. 15, p. 155 420, 2011.

[5] Q. Luo, "The elementary electronic properties of graphene," *Department of Physics and Astronomy, University of Tennessee*, 2010.

[6] P. Avouris, "Graphene: Electronic and photonic properties and devices," *Nano letters*, vol. 10, no. 11, pp. 4285–4294, 2010.

[7] F. Schwabl, *Quantum mechanics*. Springer Science & Business Media, 2007.

[8] A. De Martino, L. Dell'Anna, and R. Egger, "Magnetic confinement of massless dirac fermions in graphene," *Physical review letters*, vol. 98, no. 6, p. 066 802, 2007.

[9] I. S. Gradshteyn and I. M. Ryzhik, *Table of integrals, series, and products*. Academic press, 2014.

[10] E. Illes and E. Nicol, "Klein tunneling in the α- t 3 model," *Physical Review B*, vol. 95, no. 23, p. 235 432, 2017.

[11] F. Bouhadida, L. Mandhour, and S. Charfi-Kaddour, "Magnetic fabry-pérot interferometer for valley filtering in a honeycomb-dice model," *Physical Review B*, vol. 102, no. 7, p. 075 443, 2020.

[12] B. Aufray, A. Kara, S. Vizzini, *et al.*, "Graphene-like silicon nanoribbons on ag (110): A possible formation of silicene," *Applied Physics Letters*, vol. 96, no. 18, p. 183 102, 2010.

[13] N. Drummond, V. Zolyomi, and V. Fal'Ko, "Electrically tunable band gap in silicene," *Physical Review B*, vol. 85, no. 7, p. 075 423, 2012.

[14] X.-T. An, Y.-Y. Zhang, J.-J. Liu, and S.-S. Li, "Quantum spin hall effect induced by electric field in silicene," *Applied Physics Letters*, vol. 102, no. 4, p. 043 113, 2013.

[15] F. Li and Q. Zhang, "Valley-dependent electronic transport in quantum hall systems of α-t3 model," in *Journal of Physics: Conference Series*, IOP Publishing, vol. 1978, 2021, p. 012 011.

[16] X. Zhou and G. Jin, "Silicene-based π and φ 0 josephson junctions," *Physical Review B*, vol. 95, no. 19, p. 195 419, 2017.